Coseismic landsliding estimates for an Alpine Fault earthquake and the consequences for erosion of the Southern Alps, New Zealand

T.R Robinson[a,b] **–** corresponding author, email: tom.robinson@durham.ac.uk**;** tel: (+44) 07823 406824

T.R.H. Davies[a] email: tim.davies@canterbury.ac.nz

T.M. Wilson[a] email: thomas.wilson@canterbury.ac.nz

C. Orchiston[c] email: caroline.orchiston@otago.ac.nz

[a]Department of Geological Sciences, University of Canterbury, Private Bag 4800, Christchurch 8140, New Zealand

[b]Institute of Hazard, Risk and Resilience, Durham University, South Road, Durham, DH1 3LE, UK

[c]Centre for Sustainability, University of Otago, PO Box 56, Dunedin, New Zealand

HIGHLIGHTS

- Spatial distribution of landslide hazard for an M_w 8.0 Alpine Fault earthquake is modelled
- 28% probability of such an earthquake in the next 50 years
- 30,000 – 70,000 landslides are anticipated with 0.2–1.7 km^3 total volume
- Average landslide densities expected to be 2–9 landslides km^{-2}
- Alpine-fault-related erosion in N and S catchments is equivalent to 10–70 years aseismic erosion
- Alpine-fault-related erosion in central Southern Alps is <10 years' worth of aseismic erosion

Abstract

Landsliding resulting from large earthquakes in mountainous terrain presents a substantial hazard and plays an important role in the evolution of mountain ranges. However estimating the scale and effect of landsliding from an individual earthquake prior to its occurrence is difficult. This study presents first order estimates of the scale and effects of coseismic landsliding resulting from a plate boundary earthquake in the South Island of New Zealand. We model an M_w 8.0 earthquake on the Alpine Fault, which has produced large (*M* 7.8–8.2) earthquakes every 329 ± 68 years over the last 8 ka, with the last earthquake ~300 years ago. We suggest such an earthquake could produce ~50,000 ± 20,000 landslides at average densities of 2–9 landslides km^{-2} in the area of most intense landsliding. Between 50% and 90% are expected to occur in a 7,000 km^2 zone between the fault and the main divide of the Southern Alps. Total landslide volume is estimated to be 0.81 +0.87/-0.55 km^3. In major northern and southern river catchments, total landslide volume is equivalent to up to a century of present-day aseismic denudation measured from suspended sediment yields. This suggests that earthquakes occurring at century-timescales are a major driver of erosion in these regions. In the central Southern Alps, coseismic denudation is equivalent to less than a decade of aseismic denudation, suggesting precipitation and uplift dominate denudation processes. Nevertheless, the estimated scale of coseismic landsliding is considered to be a substantial hazard throughout the entire Southern Alps and is likely to present a substantial issue for post-earthquake response and recovery.

Keywords: Coseismic landsliding; Erosion; Denudation; Alpine Fault; Earthquakes; New Zealand

1. Introduction

Large earthquakes in mountains present a substantial hazard as a result of the cascading geomorphic effects that result from strong ground shaking (**Hewitt et al., 2008**, **Robinson and Davies, 2013**). The most obvious and widespread of these effects is coseismic landsliding, which can equal or even exceed hazards from the initial earthquake. Historic earthquakes have caused sufficient landsliding to offset or outweigh coseismic uplift (**Parker et al., 2011; Li et al., 2014**). Subsequent fluvial remobilisation of landslide material can have dramatic consequences in the form of aggradation on alluvial fans (e.g. **Davies et al., 2005**) and the infilling of reservoirs. Assessing the potential scale of coseismic landsliding is therefore a vital component of hazard assessments and of understanding mountain-building and denudation processes. Finding ways to quantitatively assess the magnitude of coseismic landsliding can therefore allow better understanding of the hazard mountainous earthquakes present, as well as their effect on mountain evolution.

Since the 1950s a number of methods have been proposed to assess the stability of slopes during earthquakes (e.g. **Newmark, 1965**; **Miles and Keefer, 2000**; **Stewart et al., 2003**). Most require relatively complete (i.e. >90% of total landslides identified) historic landslide inventories; however, such data are unavailable in most regions. Consequently, both probabilistic (e.g. **Del Gaudio and Wasowski, 2004**) and deterministic (**Kritikos et al., 2015)** approaches have been developed that can be applied without such data. In regions lacking historic inventories but with known seismic hazard, such approaches allow coseismic landslide hazard (the likelihood of a landslide occurring as a result of an earthquake) to be estimated where it was not previously possible. However, such modelling has not typically focussed on the scale of landsliding that results, and consequently attempts to estimate the scale prior to an earthquake have been limited to simple empirical relationships (e.g. **Keefer, 1984; Malamud et al., 2004**). Such relationships have limitations as they consider only seismic properties and not the environment in which the earthquake occurs, resulting in estimates with large associated errors (e.g. **Robinson and Davies, 2013**). Developing a means to estimate the potential scale of landsliding directly from a hazard model may therefore allow better and more robust hazard analyses that are crucial for risk assessments. To our knowledge, no such attempts have been undertaken previously.

One environment requiring such analysis is the Southern Alps in New Zealand, where a number of large (M > 7) earthquakes have occurred historically (**Robinson and Davies, 2013**) but there are no accurate landslide inventories compiled on Geographic Information Systems (GIS) from high resolution satellite/aerial photographs. The Southern Alps are bounded to the west by the plate boundary Alpine Fault (**Fig. 1**), which is late in its seismic cycle and capable of producing M_w 8.0+ earthquakes (**Berryman et al., 2012**). Over the last 8 ka, the fault has had an average recurrence interval of 329 ± 68 years (**Berryman et al., 2012**), with the last earthquake occurring ~300 years ago (**Yetton, 1998**). Consequently there is an estimated 28% conditional probability of the fault rupturing in the next 50 years (**Biasi et al., 2015)**. Evidence of pre-historic Alpine Fault earthquakes suggests these have all involved rupture lengths >300 km and measured horizontal displacements of 7–8 m, corresponding to M_w 7.8–8.2 (**Yetton, 1998**; **Wells and Goff, 2007; Berryman et al., 2012**; **De Pascale and Langridge, 2012**; **De Pascale et al., 2014**). These are thought to have caused widespread landsliding throughout the entire Southern Alps (**Bull, 1996**; **Berryman et al., 2001**; **Davies and Korup, 2007**), highlighting the need for pre-event estimates of the scale and extent of coseismic landsliding possible.

This study attempts a first-order model of the coseismic landsliding resulting from an Alpine Fault earthquake scenario. Landsliding is explored in terms of spatial distribution of hazard and the total landslide number and volume. A scenario approach provides an opportunity to inform planning and decision-making by relevant agencies, as well as to investigate the environmental effects from a single earthquake prior to its occurrence. Given the likelihood of an Alpine Fault earthquake, this work is vital for earthquake disaster risk management in New Zealand. The approach undertaken herein contains a number of assumptions and potentially large errors; nevertheless, such an initial attempt is necessary to formulate a basic understanding and highlight potential future avenues of research.

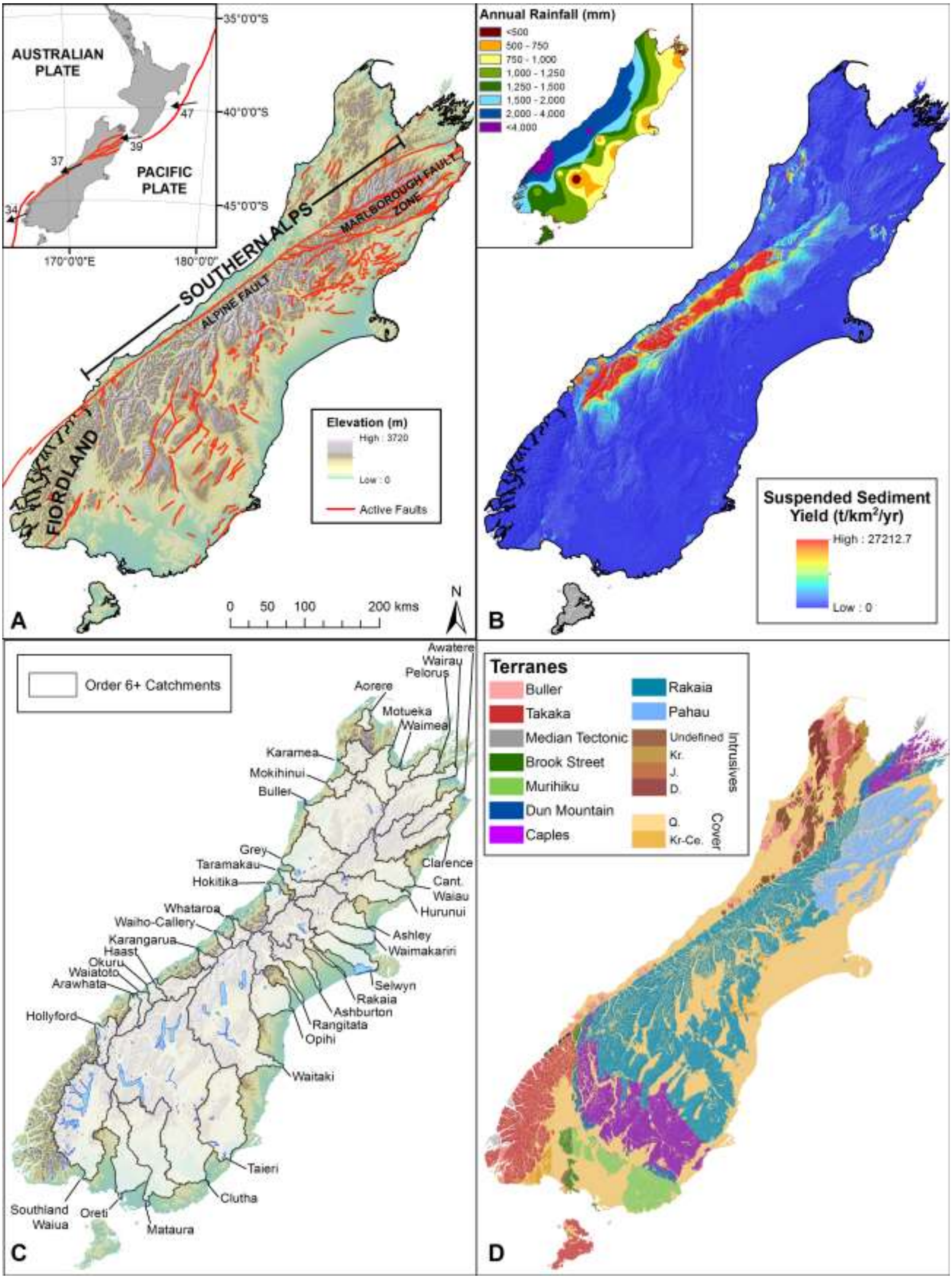

AUSTRALIAN PLATE
PACIFIC PLATE
35°0'0"S
40°0'0"S
45°0'0"S
170°0'0"E
180°0'0"
47
39
37
34
SOUTHERN ALPS
MARLBOROUGH FAULT ZONE
ALPINE FAULT
FIORDLAND
Elevation (m)
High : 3720
Low : 0
Active Faults
0 50 100 200 kms
N
A
Annual Rainfall (mm)
<500
500 - 750
750 - 1,000
1,000 - 1,250
1,250 - 1,500
1,500 - 2,000
2,000 - 4,000
<4,000
Suspended Sediment Yield (t/km2/yr)
High : 27212.7
Low : 0
B
Order 6+ Catchments
Awatere
Wairau
Pelorus
Aorere
Motueka
Waimea
Karamea
Mokihinui
Buller
Grey
Taramakau
Hokitika
Clarence
Cant. Waiau
Hurunui
Whataroa
Waiho-Callery
Ashley
Waimakariri
Karangarua
Haast
Okuru
Waiatoto
Arawhata
Selwyn
Rakaia
Ashburton
Rangitata
Opihi
Hollyford
Waitaki
Taieri
Clutha
Southland Waiua
Oreti
Mataura
C
Terranes
Buller
Takaka
Median Tectonic
Brook Street
Murihiku
Dun Mountain
Caples
Rakaia
Pahau
Undefined
Kr.
J.
D.
Intrusives
Q.
Kr-Ce.
Cover
D

Fig. 1. Tectonics, geology, and geomorphology of the South Island of New Zealand. A) Active onshore faults. Inset: tectonic setting of New Zealand showing plate boundary. B) Erosion rates in the form of suspended sediment yield (**Hicks et al., 1996**). Inset: average annual rainfall for the South Island between 1971 and 2000 (from www.niwa.co.nz). C) Major (order 6+) river catchments. d) Geologic map (after **Rattenbury and Isaac, 2012**).

2. Regional setting

2.1. Tectonics

New Zealand is situated on the boundary between the Australian and Pacific tectonic plates (**Fig. 1A**), where present day relative plate motions are some of the fastest in the world (**Norris and Cooper, 2001**). The onshore segment of the plate boundary is formed by the Alpine Fault, which runs for >600 km through the South Island. During the last 7–10 Ma the fault has accommodated ~480 km of lateral displacement (**Wellman, 1955**) and 21–25 km of uplift (**Cooper, 1980**; **Kamp et al., 1989**). Uplift rates vary along the fault from ~2.5 mm yr^{-1} in the north, to ~0 mm yr^{-1} in the south, with a peak of ~12 mm yr^{-1} in the centre (**Norris and Cooper, 2001**). This uplift has resulted in the formation of the Southern Alps (**Fig. 1A**), which presently have an average elevation of ~1,000–1,500 m and a maximum of 3,724 m at Aoraki/Mt Cook. Rapid uplift coupled with high precipitation makes the central Southern Alps some of the fastest-eroding mountains on earth, with regional erosion and uplift rates in overall dynamic equilibrium since the late Quaternary period (**Adams, 1980**).

2.2. Geology and geomorphology

The central and northern Southern Alps are composed primarily of heavily weathered greywacke and schist of the Torlesse, Rakaia and Pahau terranes (**Fig. 1D**). West of the fault, granitic basement (Buller and Takaka terranes), which has been displaced >400 km to the northeast relative to eastern terranes, is generally covered by thick Quaternary deposits (**Rattenbury and Isaac, 2012)**. Differences in lithology and uplift rates mean the Southern Alps form high mountains with deeply incised river valleys, while Fiordland has somewhat lower mountains with steep cliff faces and glaciated landforms.

Landsliding in New Zealand has typically taken the form of multi-landslide events (rather than individual landslides) initiated by heavy rainstorms or earthquakes (**Crozier, 2005**). They have involved the simultaneous occurrence of thousands to tens of thousands of landslides across areas >20,000 km^2, with median landslide densities of 30 landslides km^{-2} and maximum densities up to 100 landslides km^{-2} (**Crozier, 2005**). The largest recorded individual coseismic landslide in the South Island was the 55 million m^3 Falling Mountain landslide that occurred during the 1929 Arthur's Pass earthquake (**Korup et al., 2004**). However, individual prehistoric landslides with volumes up to 1 km^3 such as the John O'Groats deposit, are also inferred to have a coseismic (probably Alpine Fault) origin. (**Hancox and Perrin, 1994**).

2.3. Sediment supply

Suspended sediment yield (*SSY*, measured in t km^{-2} yr^{-1}) data (**Fig. 1B**; **Hicks et al., 1996**) show that short-term (decadal) erosion is highest in the central Southern Alps, where annual rainfall is extremely high (up to 15,000 mm yr^{-1}) and uplift rates are at a maximum. Suspended sediment is thought to account for ~50% of total river sediment capacity (**Davies and McSaveney, 2006**), although **Griffiths (1979)** suggested a higher proportion (~90%). When integrated across a given area, *SSY* gives the total suspended sediment contributed by that area measured in t yr^{-1}. Thus, total annual sediment removed, S_v (m^3 yr^{-1}), can be estimated from:

$$S_V = 2SSY/\rho \quad (1)$$

where ρ is the solid density of suspended sediment in t m^{-3}, and the factor 2 accounts for *SSY* representing 50% of total sediment capacity. ρ is inferred to be 2.5 t m^{-3}, corresponding to the density of the schist and greywacke that comprise the majority of the Southern Alps and contribute the majority of suspended sediment.

Denudation is notably higher in west-draining river catchments, particularly in the central Southern Alps, where it can exceed 10 mm yr^{-1} (**Table 1**). With the Southern Alps thought to be in (large-scale and long-term) dynamic equilibrium, the approximate match between calculated denudation rates and uplift rates supports the initial assumption that suspended sediment accounts for half of total load. **Cogez et al. (2015)** used offshore sediment cores to suggest long-term denudation in west-draining catchments has matched uplift during both glacial and interglacial cycles, and suggested that these short-term denudation rates have likely been consistent over the last 10–100 ka. **Wells and Goff (2007)** and **Howarth et al. (2012, 2014)** identified a > 40 year-long `sediment pulse' following major earthquakes on the Alpine Fault, suggesting substantial volumes of sediment are delivered to major river catchments as a result of Alpine Fault earthquakes. Denudation rates between major earthquakes were relatively invariable, however, suggesting the *SSY*-derived background rates represent aseismic (i.e. rainfall derived) erosion. It is not currently known what proportion of the total denudation these pulses of erosion following Alpine Fault earthquakes contribute. We attempt to answer this herein.

Table 1. Annual suspended sediment yield (*SSY*) and resulting denudation rates for the South Island order 6 or greater river catchments (see **Fig. 1**).

[a]Area of the most recent Quaternary units in each catchment from **Rattenbury and Isaac (2012)**

[b] $= \left(\frac{2SSY}{\rho}\right) / (\text{Total catchment area} - \text{Depositional area})$

Catchment	East/West Draining	Total catchment area (km^2)	Depositional area (km^2)[a]	*SSY* (kt yr^{-1})	Denudation rate (mm yr^{-1})[b]
Aorere	W	365.4	14.7	36.0	0.1
Arawhata	W	930.6	83.2	7,291.4	6.9
Ashburton	E	1,600.0	83.2	311.9	0.2
Ashley	E	1,149.8	93.6	83.7	0.1
Awatere	E	1,574.5	79.5	201.6	0.1
Buller	W	6,379.6	378.7	2,824.9	0.4
Clarence	E	3,300.7	184.3	648.3	0.2
Clutha	E	20,608.3	1,240.0	9,045.5	0.4
Grey	W	3,948.8	466.6	2,365.8	0.5

Haast	W	1,355.6	84.5	5,950.7	3.7
Hokitika	W	1,066.6	200.0	6,329.2	5.8
Hollyford	W	1,129.9	192.5	1,991.2	1.7
Hurunui	E	2,669.4	246.2	1,050.6	0.3
Karamea	W	1,211.7	41.9	149.4	0.1
Karangarua	W	408.2	27.4	2,499.4	5.3
Mataura	E	5,357.8	381.9	690.6	0.1
Mokihinui	E	7,513.6	22.7	285.4	0.3
Motueka	E	20,579.3	84.2	346.0	0.1
Okuru	W	467.9	45.7	3,120.4	5.9
Opihi	E	2,375.9	210.0	163.4	0.1
Oreti	E	3,513.2	516.6	259.5	0.1
Pelorus	E	891.1	25.4	236.9	0.2
Rakaia	E	2,830.4	445.1	4,510.2	1.5
Rangitata	E	1,816.1	298.6	1,627.0	0.9
Selwyn	E	2,027.1	415.4	144.0	0.1
Taieri	E	5,702.8	366.8	326.4	<0.1
Taramakau	W	1,002.9	186.7	2,194.4	2.2
Waiatoto	W	529.1	39.1	4,286.5	7.0
Waiau (Cant.)	E	3,330.7	382.0	2,806.5	0.8
Waiau (South.)	E	8,217.2	814.8	1,287.7	0.1
Waiho-Callery	W	290.3	58.4	3,404.3	11.7
Waimakariri	E	3,608.9	589.1	3,143.2	0.8
Waimea	E	771.1	52.6	108.7	0.1
Wairau	E	3,582.0	318.6	808.4	0.2
Waitaki	E	11,887.7	820.3	3,339.7	0.2
Whataroa	W	593.5	65.3	4,834.8	7.3

3. Methods

3.1. Coseismic landslide modelling

Assessing coseismic landslide hazard requires a method that can be applied to New Zealand without the need for historical landslide inventories, which do not exist. **Kritikos et al. (2015)** demonstrated that combining data from multiple coseismic landslide inventories in different locations could identify common effects from pre-disposing factors that could be used to model landslide hazard in other environments. They statistically analysed the locations of individual landslides in the 1994 Northridge and 2008 Wenchuan earthquakes, finding strong correlation between shaking intensity, slope angle and position, distance from active faults and streams, on the occurrence of landslides in both locations. By modelling the effect of each pre-disposing factor on landslide occurrence using fuzzy logic in GIS, they successfully reproduced the spatial distribution of landslides in the 1999 Chi-Chi earthquake. **Kritikos et al. (2015)** therefore suggested that such an approach could be utilised to assess coseismic landslide hazards in regions without historical data, using only a digital elevation model (DEM) and scenario shake-map. This assumes the modelled effects of each predisposing factor are similar in the area of interest. Consequently they could not include the influence of factors such as lithology in order to allow their method to be applied beyond Northridge and Wenchuan.

Fuzzy logic is an adaption of classical set theory, and allows a user to define membership curves which establish the degree to which changes in a pre-disposing factor influence landslide occurrence. Thus, modelling changes in these factors throughout a given study area provides information on the rate of landsliding expected for a given scenario in the same area. Combining these memberships for multiple factors on a cell-by-cell basis therefore effectively defines the likelihood (0–1) of a landslide occurring in that cell (**Fig. 2**). If the probability of the precise earthquake scenario is known, this can be included in the likelihood calculations to give ‘absolute likelihood’ of coseismic landslide occurrence. However, whilst the probability of an earthquake on a given fault in a given time frame can be known (e.g. **Biasi et al., 2015**), the probability of a specific earthquake scenario cannot, as there are effectively an infinite number of possible scenarios. When applied to a precise scenario, landslide likelihoods are therefore considered ‘relative likelihood’ i.e.

they are only associated with the scenario considered. Thus, a value of 1 signifies that landsliding is certain only in the given earthquake scenario, and 0 signifies that landsliding never occurs in the same scenario.

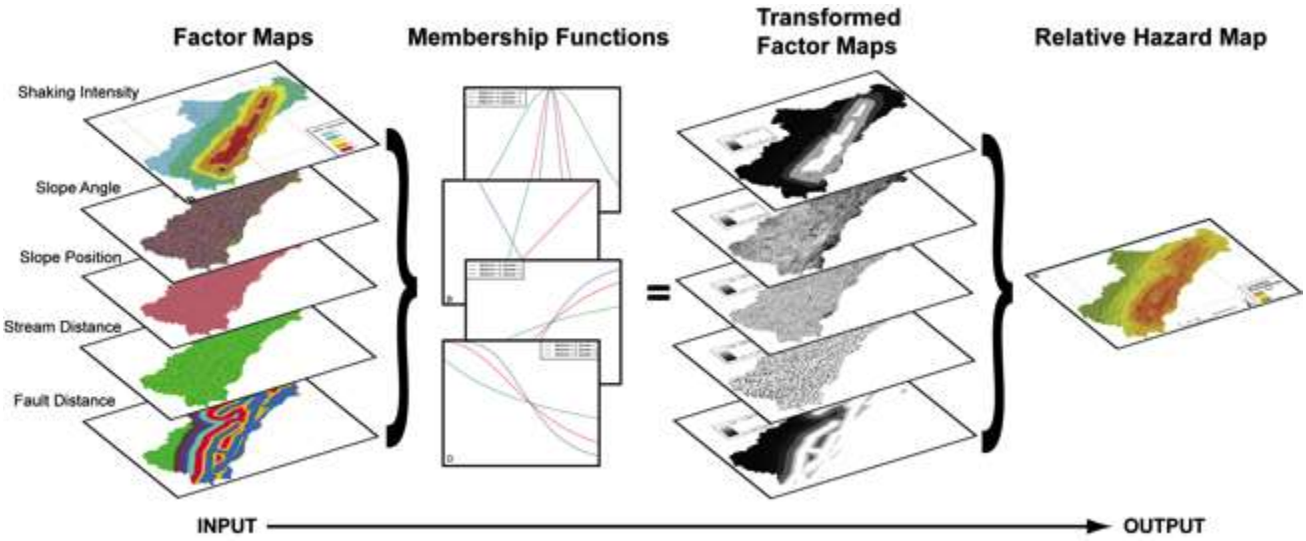

Fig. 2. Simplified workflow for producing relative coseismic landslide hazard map for scenario earthquakes. After **Kritikos et al. (2015)**.

3.2. Deriving the scale of landsliding

3.2.1. Landslide number

Estimating the number of landslides expected from a landslide hazard map is one way of quantifying the potential scale of landsliding. However, this is difficult as hazard values (*h*) do not denote whether or not a landslide will occur, but only the relative likelihood of occurrence for that scenario. Nevertheless, earthquake scenarios that produce large areas of high hazard would generally be expected to produce more landslides. Calculating landslide density for particular hazard values from historic events can therefore allow first-order estimation of landslide scale for scenario events.

We partition the hazard maps from the Northridge, Wenchuan, and Chi-Chi events in **Kritikos et al. (2015)** and two recent Fiordland earthquakes modelled below (**Figs. 3 and 4**), into 10 linear bins (0–0.1, 0.1–0.2, 0.2–0.3 etc.) and assess the density of landsliding observed in each bin for all earthquakes (**Table 2**). Using linear bins allows landslide densities to be directly compared across different historic events. Calculating the mean densities and associated one and two standard errors for each bin allows a possible range of landslide numbers to be estimated for any given hazard map based on observed events. Ideally, Bayesian statistics would be applied to estimate the distribution of densities within an individual bin; however, selecting a suitable probability distribution from a small sample set of earthquakes (five) is difficult, and risks introducing aleatoric uncertainty that cannot be accounted for and may unduly influence the results. Consequently, we use the standard error of the mean to define plausible limits on the landslide density in each bin with 1 standard error giving 68% confidence and 2 standard errors giving 95% confidence (**Table 3**).

Table 2. Landslide densities (landslides km^{-2}) observed in five historic landslide inventories for each hazard bin and the resulting sample mean ($\bar{x}$) and standard errors ($\sigma_{\bar{x}}$). NA - not available; corresponding hazard value not present (zero demonstrates the hazard class is present but no observed landslides occurred in that bin). See Section 4 (Results) for data on the 2003 and 2009 Fiordland earthquakes.

[a] After **Kritikos et al. (2015)**.

Earthquake	Hazard bin									
	$h < 0.1$	$0.1 \le h < 0.2$	$0.2 \le h < 0.3$	$0.3 \le h < 0.4$	$0.4 \le h < 0.5$	$0.5 \le h < 0.6$	$0.6 \le h < 0.7$	$0.7 \le h < 0.8$	$0.8 \le h < 0.9$	$h \ge 0.9$
Northridge[a]	0	0	0	0.001	0.016	0.134	0.604	2.621	8.144	21.289
Chi-Chi[a]	0	0	0	0.001	0.015	0.054	0.342	2.230	8.154	21.394
Wenchuan[a]	0	0	0.008	0.050	0.195	0.589	0.808	1.885	4.787	8.919
Fiordland (03)	0	0	0	0.001	0.002	0.033	0.027	0.034	0.028	0
Fiordland (09)	0	0	0	0	0.002	0.013	0.031	0.083	0.058	NA
$\bar{x}$	0	0	0.002	0.010	0.046	0.164	0.362	1.369	4.234	12.900
$\bar{x} + \sigma_{\bar{x}}$	0	0	0.004	0.020	0.083	0.272	0.517	1.917	6.052	18.103
$\bar{x} + 2\sigma_{\bar{x}}$	0	0	0.006	0.030	0.121	0.381	0.672	2.465	7.869	23.304
$\bar{x} - \sigma_{\bar{x}}$	0	0	0	0.001	0.008	0.056	0.208	0.822	2.416	5.202
$\bar{x} - 2\sigma_{\bar{x}}$	0	0	0	0	0	0	0.053	0.274	0.598	2.496

3.2.2. Total landslide volume

Calculating total landslide volume is important for evaluating erosion and denudation resulting from an earthquake scenario (see **Li et al., 2014**) and gives a better account of the scale of landsliding than a number alone. However, estimating landslide volumes is difficult when dealing with a large number of individual landslides, especially when attempting to estimate volume prior to an event. Therefore, more empirical approaches are typically undertaken (e.g. **Guzzetti et al., 2009**), which require a large number of assumptions and involve large errors, but are nevertheless useful for first order estimations in initial analyses such as our study.

Brunetti et al. (2009) analysed 19 landslide datasets resulting from a variety of different triggers on Earth (subaerial and submarine) and other planetary bodies. They showed that the cumulative probability density, $p(V_L)$ of any given landslide having a particular volume, V_L measured in m^3, followed a negative power law with a slope (i.e. average component value, β) ~ -1.3 (+0.6/-0.3):

$$p(V_{\mathrm{L}}) = kV^{-1.3} \tag{2}$$

where k defines the intercept, i.e. the value of the power-law at V = 1. This behaviour was independent of lithology, slope morphology, environment, triggering mechanism, length of period, and extent of area covered by each dataset. A Monte Carlo analysis, in which random numbers between 0 and 1 are selected from a uniform distribution to represent $p(V_L)$ for each landslide within a dataset, can therefore be used to estimate likely total volume for that dataset. For example, from the uniform distribution, values >0.9 should only be selected 10% of the time assuming a suitably large sample size, and thus when mapped onto $p(V_L)$, they will account for only the top 10% of landslide volumes.

If a random number, *RAND*, is considered to represent the probability that V_L is less than or equal to some value V' for each landslide in a dataset, such that:

$$RAND = 1 - P(|V_{\mathrm{L}} \geq V'|) \tag{3}$$

$$= 1 - \int_{V'}^{\infty} k\, V_{\mathrm{L}}^{-1.3}\, \mathrm{d}V \quad (4)$$

then it is possible to calculate individual landslide volumes for any given number of landslides. Taking a range to infinity is necessary as the limit on maximum potential landslide volume is thought to be very large but remains unknown. In practice this is unworkable and effectively makes **Eq. (4)** unsolvable. Setting an upper bound on maximum landslide volume allows *V’* to be calculated. Herein, we set this upper limit at 1 km^3. **Brunetti et al. (2009)** noted that the occurrence of landslides >1 km^3 may not be accurately represented by **Eq. (2)** due to the rarity of their occurrence. Setting this upper limit is appropriate for first order assessments, but it should be noted that the results should consequently be considered as minimum values. Total landslide volume, V_{LE}, for any dataset can therefore be calculated from:

$$V_{\mathrm{LE}} = \sum_{i=1}^{n} V_i' \quad (5)$$

where *n* is the total number of landslides and *V’* is calculated for each landslide, *i*, from:

$$RAND = 1 - \int_{V'}^{10^9} k\, V^{-1.3}\, \mathrm{d}V \quad (6)$$

To obtain *k*, **Eqs. (5) and (6)** are applied to historic coseismic landslide events and the modelled results (V_{LE}) are compared to the observed total volumes (V_{LO}). If *k* is initially set at 1, its real value for each event can be found from the ratio between V_{LE} and V_{LO} (**Table 3**). The results suggest that, for an individual event, *k* rarely ranges over more than a single order of magnitude; however, across multiple events *k* varies by as much as three orders of magnitude (**Table 3**). We infer this to be an effect of local factors such as lithology, uplift, and weathering rates. While such factors were deemed not to affect the slope of the power law (**Brunetti et al., 2009**), they likely affect the position of the distribution on the *y*-axis. For application to scenario events in areas where the local value of *k* cannot be estimated from historic events, we suggest a conservative range of $0.001 \leq k \leq 0.1$. This allows total landslide volume to be estimated for a given number of landslides.

Table 3: Modelled (V_{LE}) and observed (V_{LO}) total landslide volumes and the corresponding range in *k* values for historic coseismic landslide events for which the total landslide number (*n*) is known (details are in Supplementary Data). Data from **Keefer (1994; 2002)**, **Malamud et al. (2004)** and **Li et al., (2014)**.

[a]Volume calculated by converting each landslide inventory area to volume using area–volume scaling relationships in the corresponding references.

Earthquake	*n*	V_{LO} (Mm^3)	V_{LE} (Mm^3) Min	Max	Range in *k*
1976 Guatemala	50000	116	16900	25400	0.005–0.007
1980 Mammoth Lakes, CA, USA	5253	12	1100	3775	0.003–0.01
1983 Coalinga, CA, USA	9389	1.94	2439	5706	0.0003–0.0008
1986 San Salvador, El Salvador	216	0.378	1.78	480	0.0008–0.2
1989 Loma Prieta, CA, USA	1500	74.5	100	1479	0.05–0.7
1994 Northridge, CA, USA	11111	120[a]	3007	6502	0.02–0.04
2008 Wenchuan, China	57150	2800[a]	19320	28150	0.1–0.14

4. RESULTS

4.1. Hazard modelling applicability

Before being applied to a scenario Alpine Fault earthquake, the applicability of the hazard modelling to the South Island is quantitatively tested. The performance of landslide hazard models is typically measured quantitatively via success curves, which show the predictive ability of the model (**Remondo et al., 2003**). These compare the cumulative percentage of observed landslides (*y*-axis) to the cumulative percentage of hazard values from largest to smallest (*x*-axis), which measures the percentage of true positives (i.e. the number of landslides occurring in the highest *x*% of hazard cells). To be successful, a model must achieve area under the curve (*AUC*) values >0.7, as smaller values are considered only slightly better than random chance (**Kritikos et al., 2015**).

We test the hazard model on the 2003 and 2009 Fiordland earthquakes using landslide inventories provided by GNS Science. These inventories are not suitable for more traditional statistical analysis such as linear regression (e.g. **Miles and Keefer, 2000**; **Stewart et al., 2003**) as the inventory accuracy varies up to ±500 m for landslides not directly beneath the reconnaissance flight paths. In order to account for this, cell sizes >500 m would be necessary, which is not appropriate for regional-scale modelling. Nevertheless, these inventories can be used to test the applicability of the method to the South Island. To apply the method herein, a 60 m DEM (re-sampled from the Land Information New Zealand 25 m DEM) is used along with mapped active faults (**Fig. 1**) taken from the GNS Science Active Fault Database (http://data.gns.cri.nz/af/) and streams defined using an inbuilt Flow Accumulation tool in ArcGIS with a minimum catchment area of 1 km^2. The relevant membership curves for slope angle, MM intensity, slope position, stream distance, and fault distance are taken directly from **Kritikos et al. (2015)**.

4.1.1. Historic New Zealand earthquake models

In 2003, an M_w7.2 earthquake occurred offshore of Thompson Sound in Fiordland (**Fig. 3A**) at a depth of ~20 km (**Hancox et al., 2003**). The earthquake generated a maximum of *MM* 9 shaking primarily in an uninhabited region west of Lake Te Anau (**Fig. 3A**). As a result, >400 landslides were triggered in a region extending 20–30 km from the main fault rupture zone (**Hancox et al., 2003**). Most of these occurred on slopes >35° and ranged in volume from a few cubic metres to a maximum of ~700,000 m^3. The inventory was compiled from helicopter reconnaissance flights in the week following the earthquake and was later digitised in GIS.

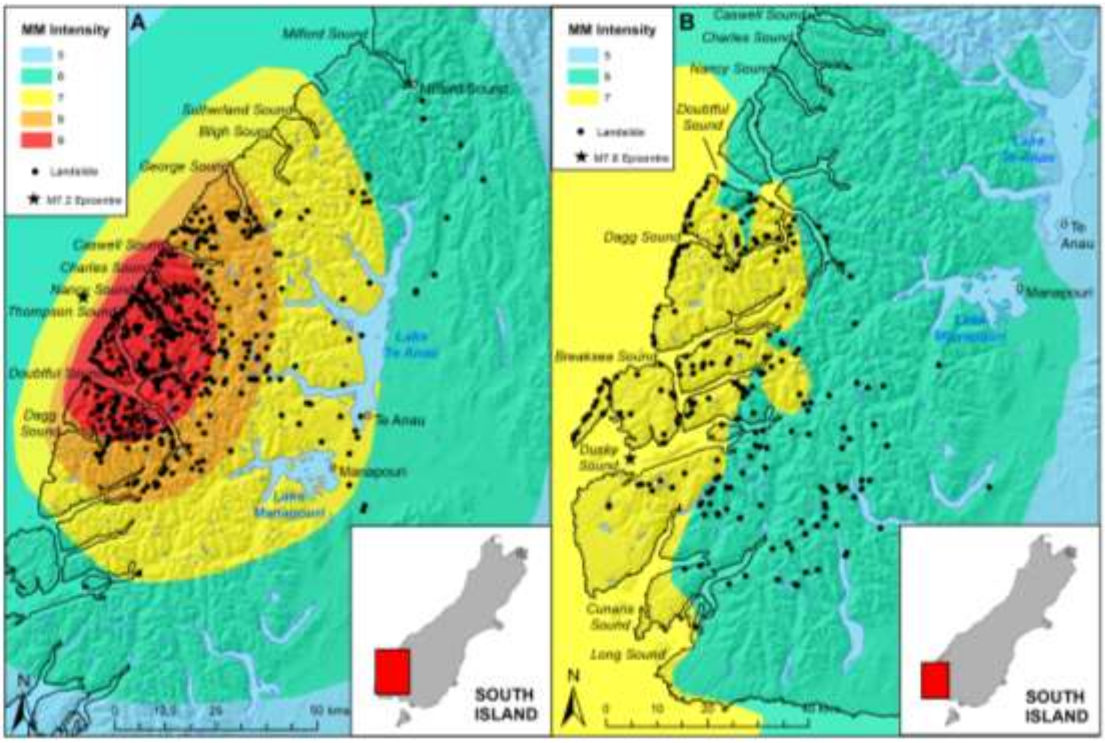

Fig. 3. Extent of landsliding and shaking intensity from the A) 2003 M_w 7.2 Fiordland earthquake and B) 2009 M_w 7.8 Fiordland earthquake.

The epicentre of the 2009 M_w 7.8 Fiordland earthquake was at the mouth of Dusky Sound (**Fig. 3B**) at a depth of ~30 km, with rupture propagating up-dip to a depth of ~15 km (**Fry et al., 2010**). Despite its large magnitude, the event generated lower onshore shaking intensities than the 2003 event (**Fig. 3**). Consequently, the earthquake produced fewer landslides (~200) than the 2003 event (**Fig. 3**). Landslide maps were compiled using the same approach as the 2003 earthquake.

The relative hazard maps for each earthquake are shown in **Fig. 4** along with the associated success curves. For the 2003 Fiordland earthquake an *AUC* value of 0.749 is achieved, corresponding to 45% of landslides in the highest 20% of hazard values. For the 2009 Fiordland earthquake an *AUC* value of 0.912 is achieved, corresponding to 90% of landslides in the highest 20% of hazard values (**Fig. 4C**). This is consistent with results for the Northridge, Wenchuan, and Chi-Chi earthquakes, where 85% (*AUC* = 0.904), 70% (0.839), and 92% (0.915) of landslides occurred in the highest 20% of hazard values respectively (**Kritikos et al., 2015**). This suggests that the model and data are applicable beyond their initial study areas. The success of the model in Fiordland, and the similarities between Taiwan and the Southern Alps particularly in terms of rapid plate motions, high seismicity, heavily vegetated and weathered terrain, and primarily schistose lithology, suggests this method can be applied for an Alpine Fault earthquake.

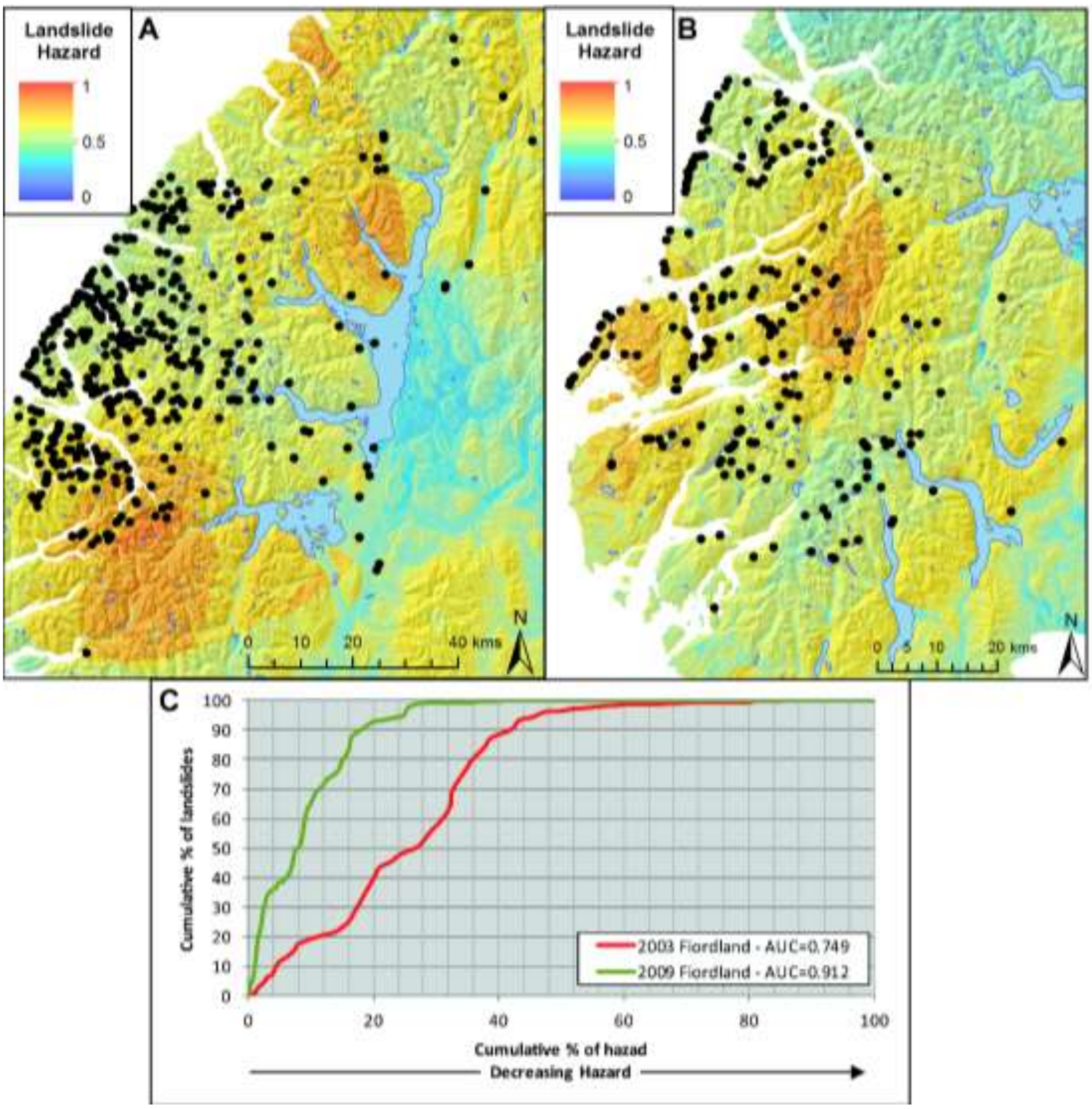

Fig. 4. Fuzzy-logic-derived coseismic landslide hazard maps for the A) 2003 Fiordland and B) 2009 Fiordland earthquakes; and C) the corresponding success curves. Note that the maximum hazard values and their extent estimated for the 2009 earthquake are lower than those estimated for the 2003 event despite the difference in earthquake magnitude. This is a result of earthquake shaking and

suggests that accurately modelling potential shaking intensities is more important for landslide hazard than correctly estimating earthquake magnitude.

4.2. Application to future earthquake scenarios: An Alpine Fault event

4.2.1. Modified Mercalli intensity modelling

The most likely scenario for an Alpine Fault earthquake is considered to be an M_w 8.0 event involving ~380 km of fault rupture between Milford Sound and the Ahaura River and maximum horizontal displacements of ~7 m (**Robinson and Davies, 2013; Robinson et al., 2014**). Isoseismal modelling for such a scenario was carried out by **Robinson et al. (2015)** using the OpenSHA software. OpenSHA calculates the shaking intensity that has a 50% likelihood of occurring (**Field et al., 2003)**. The software requires parameters such as fault dip, rake, and depth. as well as simple site data such as shear wave velocity. The data used for modelling herein are shown in **Table 4** and the resulting isoseismal model is shown in **Fig. 5**.

Table 4. Data used for modelling isoseismals for an Alpine Fault earthquake in OpenSHA. From **Robinson et al. (2015)**.

[a]Rake is measured along fault strike, rather than as absolute rake.

[b]Fault dip is divided into segments; the first comprises the northern and central segments of the fault, and the second comprises the southern (south of Haast) section of the fault (after **Barth et al., 2013**).

Data Type	**Input Data**	**Reference**
	Intensity Measure Relationships	
Intensity Measure Type	MMI	
Tectonic Region	Active Shallow Crust	
Component	Average Horizontal	
	Site Data Providers	

*Vs*30 (m s^{-1})	180.0 (Default)	
Site Data Provider	Global *Vs*30	
Digital Elevation Model	SRTM30 Version 2	
Region Type	Active Tectonic	
	Earthquake Rupture	
Rupture Type	Finite source	
Magnitude	8.0	See text
Rake[a]	172°	**Norris and Cooper, 2001**
Fault Dip[b]	60° and 82°	**Barth et al., 2013**
Fault Depth	12 km	**Beavan et al., 2010**
Fault tips	44.51S, 167.83E 42.50S, 171.85E	
Fault Type	Stirling's	**Field et al., 2003**

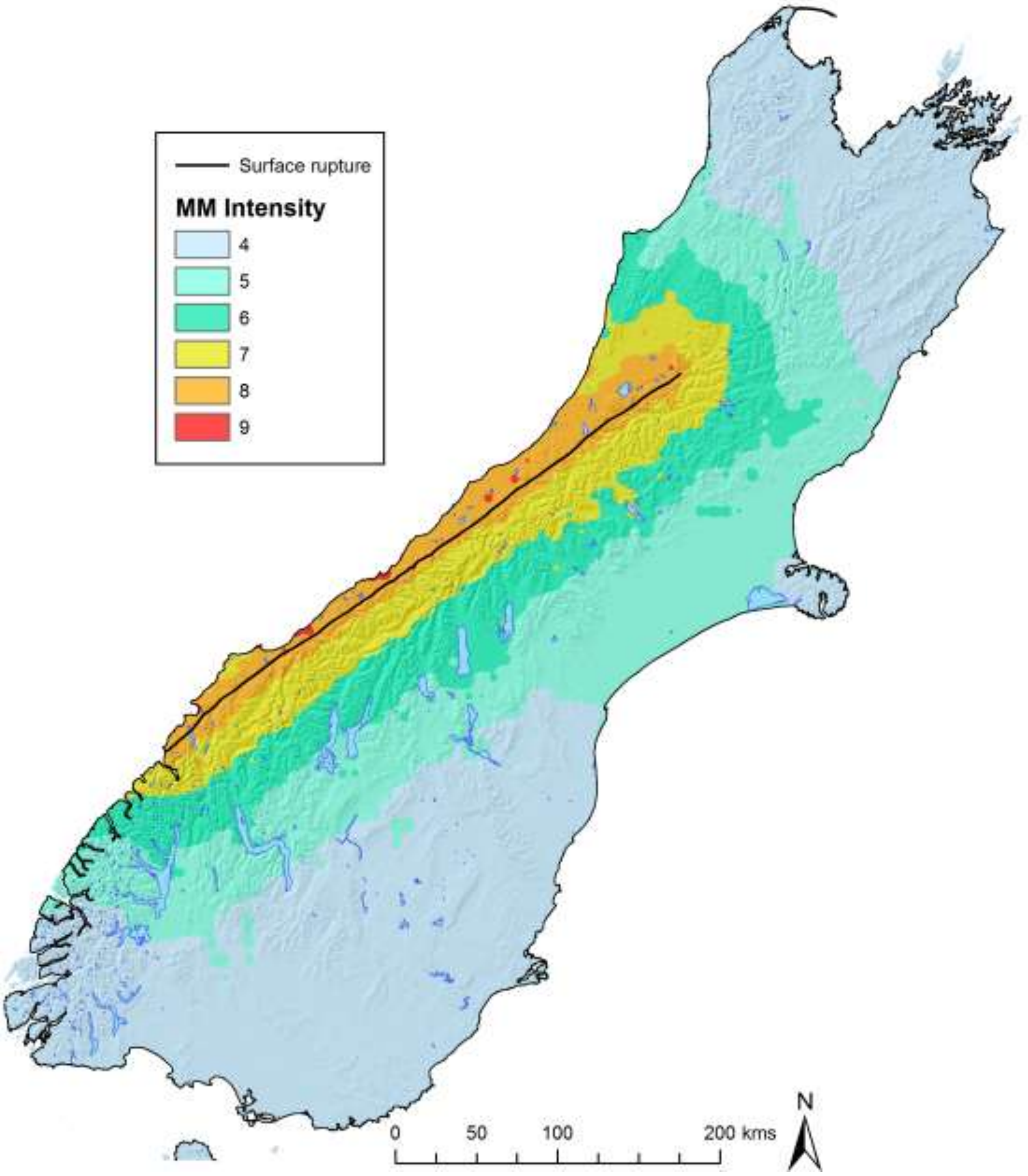

Fig. 5. Isoseismals for an M_w 8.0 Alpine Fault earthquake after **Robinson et al. (2015)**. See **Table 2** for modelling data.

4.2.2. Coseismic landslide hazard modelling

The results of applying the method of **Kritikos et al. (2015)** to this earthquake scenario are shown in **Fig. 6**. Modelled hazard values range between 0.007 and 0.969, with the highest values occurring in the central Southern Alps near to Aoraki/Mt Cook. In this region the highest hazard values occur in a narrow band between the Alpine Fault and the main divide (**Fig. 6B**). To the north high hazard values cover a larger area, extending ~20 km east of the main divide, probably resulting from the presence of several major mapped faults (**Fig. 6C**). Isolating only the highest 20% of hazard values gives a total area of ~7,000 km^2 along the entire length of the fault rupture (**Fig. 7**). Assuming this model has similar accuracy to those for the Northridge, Wenchuan, Chi-Chi and Fiordland earthquakes, we expect 50–90% of the total landslides to occur in this region.

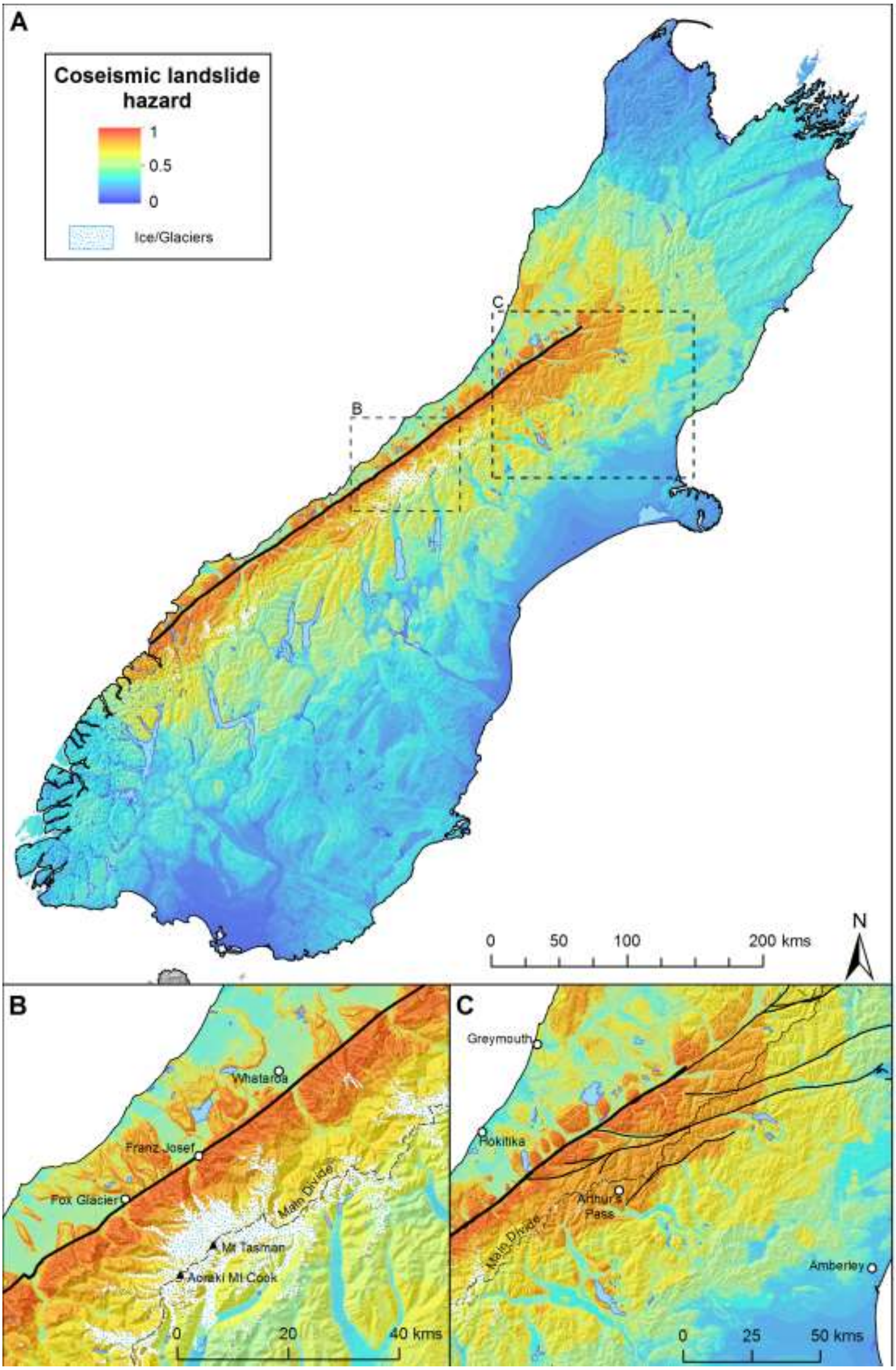

Fig. 6. Coseismic landslide hazard resulting from an M_w 8.0 Alpine Fault earthquake scenario (**Fig. 5**) for A) the entire South Island; B) the central Southern Alps; and C) the northern Southern Alps. Major mapped faults are shown in black.

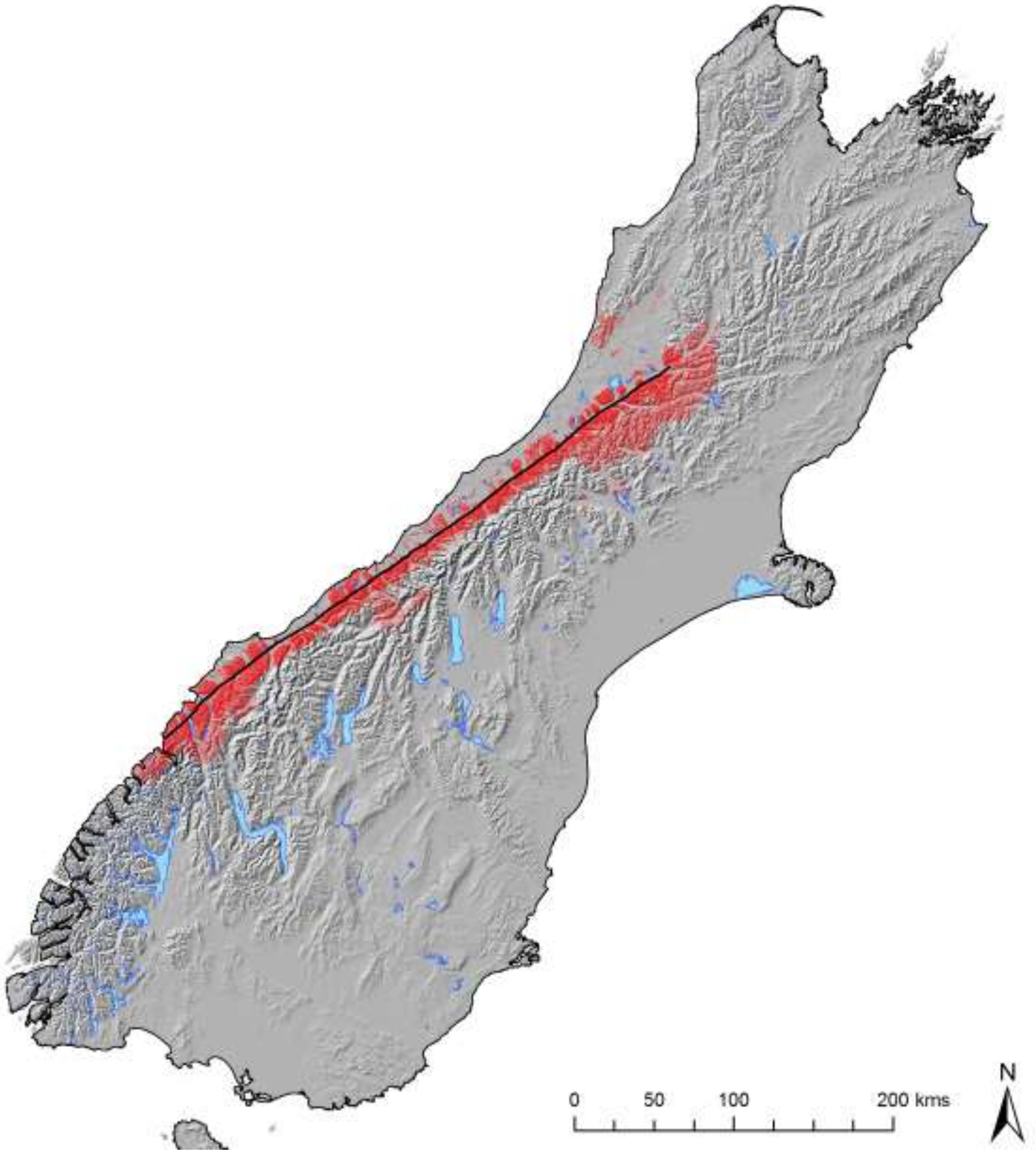

Fig 7: Spatial extent of the highest 20% of modelled coseismic landslide hazard for an M_w 8.0 Alpine Fault earthquake. This region is anticipated to experience 50–90% of the total landslides.

4.2.3 Total landslide number estimates

Once permanent ice cover and glaciers have been masked out to avoid modelling landslides in these locations, total area corresponding to each hazard bin is calculated. From the densities in **Table 2** there is 68% confidence that between

~28,000 and ~70,000 landslides would occur, and 95% confidence that between ~8,000 and ~94,000 would occur, with a mean estimate of ~50,000 landslides (**Table 5**). Average landslide density across the entire South Island is therefore between 0.19 and 0.46 landslides km^{-2} at 68%, and 0.05 and 0.60 landslides km^{-2} at 95% confidence, with a mean of 0.33 landslides km^{-2}. In the area of most intense landsliding (**Fig. 7**) however, average densities are expected between 2.0 and 9.0 landslides km^{-2} at 68% confidence, and 0.6 and 12.0 landslides km^{-2} at 95% confidence.

At the 68% confidence level, the number of landslides anticipated is similar to that observed following the Chi-Chi, Wenchuan, and Guatemala earthquakes (**Table 4**). These earthquakes present perhaps the most extreme examples of coseismic landsliding in recorded history, and this suggests that a future earthquake on the Alpine Fault could cause similar numbers of landslides.

Table 5. Area and the total number of landslides estimated to occur in each hazard bin for an M_w 8.0 Alpine Fault earthquake. See **Table 2** for data. [a]Contributing area is the total area of each bin minus the corresponding area covered by ice or glaciers.

Hazard Bin	Contributing Area (km^2)[a]	$\bar{x} - 2\sigma_{\bar{x}}$	$\bar{x}$ - $\sigma_{\bar{x}}$	$\bar{x}$	$\bar{x} + \sigma_{\bar{x}}$	$\bar{x} + 2\sigma_{\bar{x}}$
$h < 0.1$	82.5	0	0	0	0	0
$0.1 \leq h < 0.2$	17,474.5	0	0	0	0	0
$0.2 \leq h < 0.3$	37,648.9	0	0	60	121	181
$0.3 \leq h < 0.4$	38,138.2	0	25	400	774	1,148
$0.4 \leq h <$	18,730.6	0	157	859	1,561	2,264

0.5						
$0.5 \leq h < 0.6$	14,149.8	0	798	2,327	3,856	5,384
$0.6 \leq h < 0.7$	11,915.6	629	2,473	4,318	6,162	8,007
$0.7 \leq h < 0.8$	5,934.7	1,625	4,876	8,127	11,377	14,628
$0.8 \leq h < 0.9$	4,545.9	2,720	10,984	19,247	27,510	35,774
$h \geq 0.9$	1,155.9	2,885	8,898	14,911	20,925	26,938
Total	**150,932.2**	**7,859**	**28,211**	**50,249**	**72,286**	**94,324**

4.2.4. Total landslide volume estimates

Total landslide volume is estimated using 10,000 Monte Carlo trials for each of the five landslide number estimates (**Table 5)** with *k* selected randomly from a uniform distribution between 0.001 and 0.1 for each individual trial. The results of each trial are collated (shown in Supplementary Data) and presented as a frequency distribution (**Fig. 8**) illustrating the range in total volumes modelled. Modelled total volumes range between 2.32×10^{-3} and 4.44 km^3 with first, second, and third quartiles of 0.26, 0.81, and 1.68 km^3 respectively. Maximum individual landslide volumes are typically on the order of 0.1 km^3.

Interestingly, while four of the five Monte Carlo tests converged, there is notable bimodality in the results (**Fig. 8**). Tests with a total landslide number >50,000 converged on total volumes of ~2 km^3, while the test with <10,000 landslides converged on ~0.2 km^3; and the test with ~30,000 landslides did not converge (**Fig. 8**). An initial interpretation may be that once the number of landslides exceeds ~50,000, total landslide volume trends towards ~2 km^3.

For the Wenchuan earthquake, ~50% of the total landslide volume estimated by **Li et al. (2014)** came from a single giant (~1 km^3) landslide. The occurrence of one or more similar volume landslides following an Alpine Fault earthquake could dramatically increase the total volume estimates provided here; however, such events are rare (only one has been identified in the South Island; see **Hall et al., 2014** for discussion on the 27 km^3 Green Lake landslide). The total landslide volumes estimated herein are therefore speculative, with 0.81 +0.87/-0.55 km^3 considered a most likely estimate for this earthquake scenario.

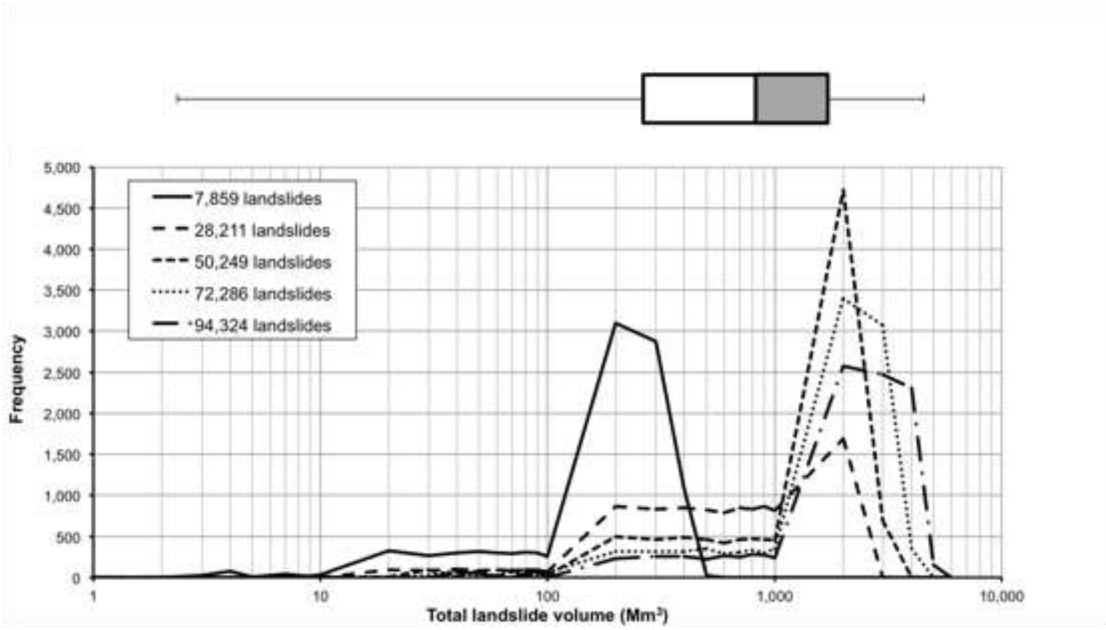

Fig. 8. Frequency distribution of modelled total landslide volumes from an Alpine Fault earthquake. Data derived from 10,000 Monte Carlo trials for each landslide number estimate (**Table 5**). Details are in Supplementary Data.

4.3. Consequent denudation

Analysing the effects of coseismic landsliding on major river catchments provides a means for assessing potential environmental impacts (**Korup et al., 2004**). Of particular interest is the amount of denudation that occurs and the amount of sediment available for aggradation within each catchment. Understanding how much denudation occurs as a result of a particular earthquake is vital to understanding mountain building processes (**Parker et al., 2011**; **Li et al., 2014**) and the medium-to-long-term response of major river systems.

Herein South Island river catchments of order 6 and larger are investigated (**Fig. 1**). Order 6 catchments likely present the smallest catchments for which meaningful results are possible, as the methods herein give greater uncertainty for smaller areas. In total, using the NIWA River Environment Classification (REC) system, there are 36 river catchments of order 6 or higher, which drain >70% of the South Island (**Table 1**). To quantify the relative impacts of landsliding between catchments, a Landslide Factor, L_F, is calculated. L_F quantifies the relative rate of landsliding per unit catchment area:

$$L_{\mathrm{F}} = (N_{\mathrm{c}i}/N_{\mathrm{T}})/(A_{\mathrm{C}i}/A_{\mathrm{T}}) \quad (7)$$

where N_{Ci} is the number of landslides in catchment i (calculated from the area of each hazard class within the corresponding catchment), N_T is the total number of landslides across the whole South Island, A_{Ci} is the area of catchment i, and A_T is the total area of the South Island. Thus, catchments with $L_F > 1$ produce more landslides per area than the South Island average, while those with $L_F < 1$ produce fewer.

Of the catchments investigated, 16 have $L_F > 1$, contributing >65% of the total landslide number despite covering just ~20% of the South Island (**Table 6**). The Taramakau, Waiho-Callery and Hollyford catchments are worst affected, with L_F ~10. This suggests that these catchments experience landslides at ~10× the average Island-wide rate.

Of the catchments with $L_F > 1$, 75% are west-draining (**Table 6**). The Canterbury Waiau is the worst affected east-draining catchment, with L_F ~ 2. While landsliding is anticipated to be greatest west of the main divide, there may also be substantial effects to the east, where most population and infrastructure are located.

4.3.1. Catchment erosion and denudation

Total landslide volumes are calculated using Monte Carlo analysis for all catchments with $L_F > 1$ (**Table 6**). Most catchments have total landslide volumes with inter-quantile ranges (Q_1–Q_3; *IQR*) of approximately 0.01–0.1 km^3, although the relatively small Waiho-Callery, Karangarua, Okuru, and Waiatoto catchments have an *IQR* value closer to 0.005–0.05 km^3 (**Fig. 9A**). The Taramakau and Hollyford catchments have broadly similar anticipated volumes to the Buller and Grey catchments (**Fig. 9A**), despite being <1/4 of the size (**Table 1**). This equates to ~10,000–100,000 m^3 km^{-2} in the Taramakau and Hollyford catchments compared to ~1,500–15,000 m^3 km^{-2} in the Buller and Grey catchments. In total 60–80% of the total Island-wide landslide debris is expected in catchments with $L_F > 1$ although they occupy just ~20% of the total South Island area.

Table 6. Total number of landslides and resulting average Impact Factor (L_F) for order 6 and above South Island (SI) river catchments.

Catchment	% total SI area	Total landslide number					Average L_F
		$\bar{x} - 2\sigma_{\bar{x}}$	$\bar{x}$ - $\sigma_{\bar{x}}$	$\bar{x}$	$\bar{x}$ + $\sigma_{\bar{x}}$	$\bar{x}$ + $2\sigma_{\bar{x}}$	
Taramakau	0.7	609	1,759	3,567	5,050	6,532	10.38
Waiho-Callery	0.2	167	458	964	1,363	1,762	9.66
Hollyford	0.7	635	1,849	3,719	5,263	6,807	9.62
Hokitika	0.7	566	1,617	3,306	4,680	6,053	9.04
Karangarua	0.3	159	460	919	1,299	1,680	6.61
Okuru	0.3	179	510	1,031	1,460	1,888	6.45
Whataroa	0.4	215	639	1,256	1,778	2,300	6.22
Grey	2.6	1,410	4,072	8,277	11,737	15,197	6.12
Arawhata	0.6	316	969	1,864	2,641	3,417	5.89
Haast	0.9	406	1,284	2,415	3,424	4,433	5.26
Waiatoto	0.4	154	437	893	1,266	1,638	4.93
Waiau (Cant.)	2.2	456	1,698	2,983	4,269	5,555	2.64
Rakaia	1.9	362	1,312	2,291	3,271	4,251	2.40
Buller	4.2	744	2,690	4,865	6,979	9,095	2.24

Waimakariri	2.4	408	1,516	2,658	3,801	4,944	2.17
Hurunui	1.8	223	855	1,527	2,200	2,873	1.67
Rangitata	1.2	55	225	428	632	837	0.67
Ashley	0.8	27	121	234	348	462	0.57
Ashburton	1.1	35	148	284	421	559	0.50
Waitaki	7.9	252	1,035	2,023	3,012	4,006	0.48
Clarence	2.2	51	247	522	797	1,073	0.43
Clutha	13.7	199	969	2,122	3,275	4,438	0.28
Waiau (South.)	5.4	64	308	690	1,073	1,460	0.23
Wairau	2.4	16	105	271	438	606	0.20
Opihi	1.6	10	62	158	254	352	0.17
Mokihinui	0.5	1	12	41	70	100	0.14
Waimea	0.5	0	11	42	72	103	0.13
Awatere	1.0	0	20	74	128	182	0.11
Selwyn	1.3	5	27	68	108	149	0.09
Motueka	1.4	0	14	62	110	159	0.07
Oreti	2.3	0	11	50	89	129	0.03

Mataura	3.5	0	8	49	91	133	0.02
Pelorus	0.6	0	1	8	15	23	0.02
Taieri	3.8	0	3	29	56	84	0.01
Karamea	0.8	0	0	6	11	17	0.01
Aorere	0.2	0	0	0	1	1	0.00
Total	72.4	7,726	25,455	49,695	71,483	93,299	1.32
South Island Total	**100.0**	**7,859**	**28,211**	**50,249**	**72,286**	**94,324**	**1.00**

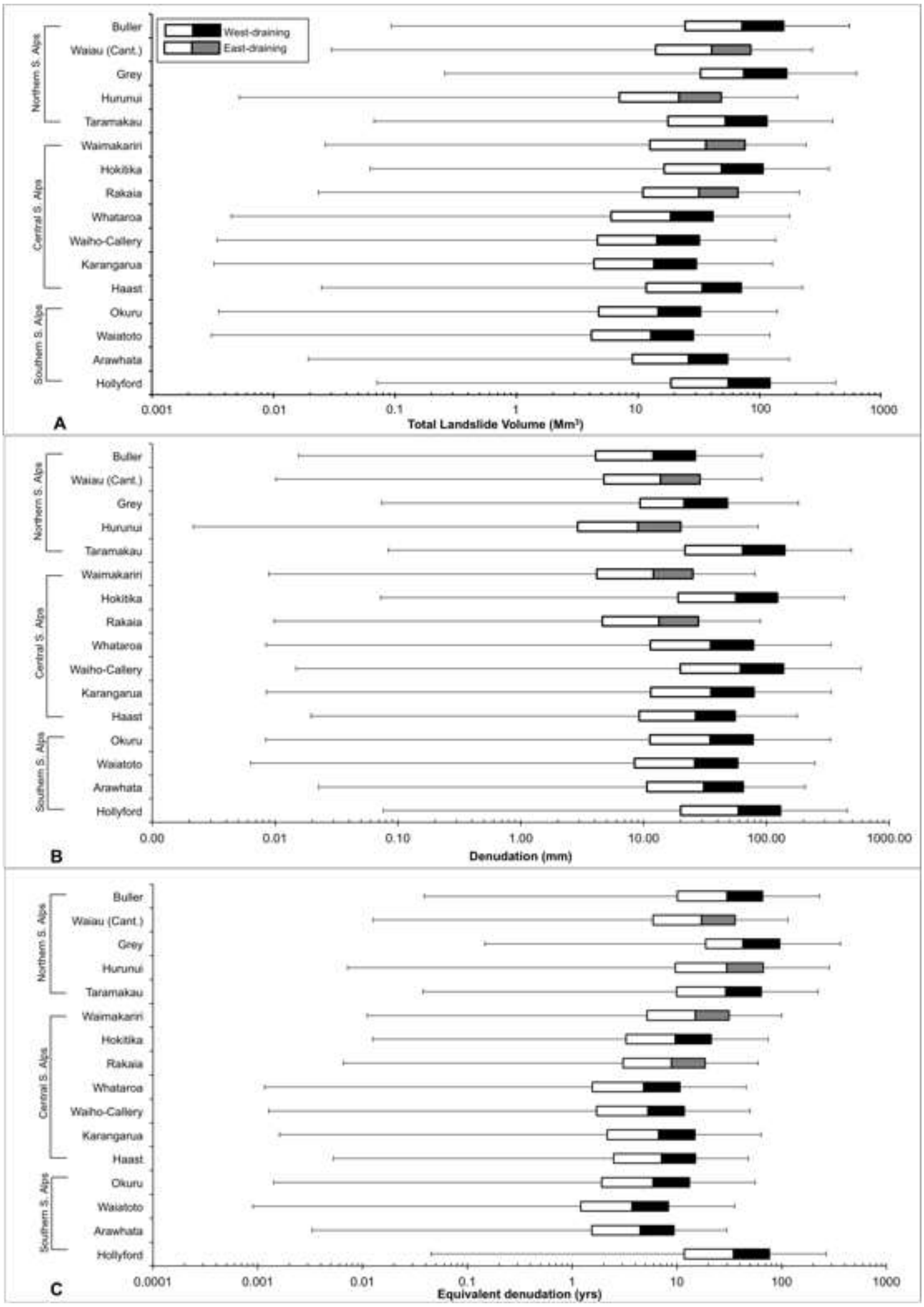

Fig. 9. Coseismic landslide impacts on individual river catchments. A) Estimated total landslide volumes; B) resulting denudation; and C) equivalent years of denudation compared to aseismically-derived background rates.

Coseismically-derived denudation is calculated for each catchment and compared to the annual aseismically-derived denudation calculated from *SSY* data (**Table 1**). Coseismic denudation is highest in the central west-draining catchments, and lowest in the east-draining catchments (**Fig. 9B**), which is broadly consistent with annual aseismic denudation (**Table 1**). The Hokitika, Taramakau, Waiho-Callery, and Hollyford catchments are anticipated to experience the highest coseismic denudation, with between 20 and 140 mm expected. Compared to annual aseismic denudation; however, coseismic denudation could account for between 10 and 70 years' worth, and possibly >100 years' worth, in the Hollyford catchment and those north of the Taramakau (**Fig. 9C**). Thus in any given 300 year period (i.e. the time between Alpine Fault earthquakes), up to 1/4 of the total erosion in these catchments results from a single Alpine Fault earthquake. With erosion rates likely to remain substantially above background rates for several years after an earthquake (**Marc et al., 2015**), it is feasible that Alpine Fault earthquakes could be responsible for between 1/3 and 1/2 of total erosion in these catchments.

These levels of erosion occur virtually instantaneously and thus have the potential to be catastrophic, because the normal river sediment transport capacity will be exceeded, and thus river behaviour will be dramatically altered. This is true even for those catchments in the central Southern Alps where coseismic erosion is estimated to be relatively small, since a short term pulse of several years' worth of sediment is still a catastrophic event.

5. Discussion

5.1. Modelling limitations

5.1.1. Model success metrics

The method for modelling landslide hazard herein has been deemed sufficient based on success curves (**Fig. 4C**). However, success curves only detail a model's ability to represent true positive and negative events, ignoring the occurrence of false positives (areas of high hazard with no landslides) and false negatives (areas of low hazard with landslides). Identifying these is equally important, as they detail the over- and under-prediction rates respectively. However, measuring these is difficult as these hazard maps do not determine whether or not a landslide will occur, rather the likelihood that one will occur. Thus, landslides occurring in cells with low hazard do not strictly represent false negatives, but rather locations where landslides were considered less likely. While the success curves therefore demonstrate that the majority of landslides occurred in cells with the highest hazard values, these hazard maps should be considered with caution, and used only for providing a regional overview of the likely scale and extent of landsliding in a given earthquake scenario.

5.1.2. Sensitivity to MM intensity

A further point to consider is the sensitivity of the model to the triggering factor; herein modelled as *MM* intensity. Because this factor has a large influence on the likelihood of a landslide occurring, it is vital that the underlying model is sufficiently accurate. Factors such as rupture propagation, fault segmentation, and surface geology are likely to affect the local shaking intensity field and therefore the likelihood of a landslide occurring. Herein *MM* intensity has been modelled at a regional level, accounting for surface geology in the form of a global shear wave velocity model to depths of 30 m (**Field et al., 2003**). Factors such as fault segmentation have not been accounted for, as the Alpine Fault is segmented on a scale of several kilometres (**Norris and Cooper, 2001**), which was considered too fine for a regional scale model. Different epicentre locations were tested in order to gauge their effect; however, this was relatively small due to the large rupture length (380 km). Nevertheless, rupture directivity may play an important role, although this is entirely dependent on the epicentre location in conjunction with the subsequent fault rupture, which is difficult to anticipate a pre-event.

5.1.3. Predisposing factors not considered

Kritikos et al. (2015) considered five predisposing factors that were independent of study area in order to produce a general model that could be applied beyond their study regions. Consequently, they ignored local factors such as lithology and soil moisture content as these are not comparable between different locations. Nevertheless, such factors have been considered important by other authors (e.g. **Keefer, 2000; Khazai and Sitar, 2004**). Thus, in locations where the effects of such factors are known, it is important to ensure they are included within the hazard modelling to produce more accurate results. However, this is not the case in New Zealand, as statistical analysis of previous landslide events has not hitherto been undertaken. While the results herein do not account for local factors, the approach taken is considered adequate for a first order modelling attempt. Such initial studies can be important for highlighting and prioritising locations requiring further study, helping to focus research on to important issues.

5.1.4. Use of landslide numbers

The results herein have focussed on the number of landslides as the test inventories utilise point data rather than polygon data. Preferably areal landslide density would be derived instead as this provides a more accurate measure of the scale of landsliding as well as total volume (e.g. **Li et al., 2014**). However, this requires all test inventories to contain consistent polygon data, which are not available for the Fiordland datasets. Consistent mapping techniques are crucial for generating accurate inventories, and for estimating the different factors that influence landslide occurrence. Hitherto, multiple mapping techniques have been used by different investigators with some plotting corresponding source zones and deposits as separate polygons while others plot these as single polygons. Further, some techniques aggregate numerous small landslides in close proximity, while others map each individual slide (**Li et al., 2014**). Modelling landslide area rather than a landslide number requires accurate data collection to produce the most consistent inventories.

5.1.5. Monte Carlo modelling

The use of Monte Carlo modelling for landslide volume has effectively reduced the ability of the model to identify extreme events. In general, the catchments with the largest number of landslides also have the largest total volumes. This is because Monte Carlo modelling in effect filters out extreme events, by converging towards an average value. It therefore ignores the possibility that large volume landslides can occur anywhere. This is an important issue as in any landsliding event a small number of large landslides cause the most significant problems. Thus a catchment can experience very few landslides, but still contribute very large debris volumes. Nevertheless, it is more likely that catchments in which more landslides occur will have a higher probability of large volume landslides. Identifying these catchments can allow future site-specific studies to investigate the potential for large volume slope failures (e.g. from geomorphic characteristics: Davies, 2014). The distributions involved in the Monte Carlo modelling have therefore been selected to represent the most realistic volume distributions based on available knowledge. Consequently, very large landslides are rarely modelled in this study as globally they are observed to be rare.

5.2. Implications for disaster risk management

The scale of landsliding suggested for an Alpine Fault earthquake herein would be amongst the most extensive worldwide, exceeding that observed in the 1994 Northridge and 1999 Chi-Chi earthquakes, and approaching the 2008 Wenchuan earthquake (**Table 3**). These results are important for disaster risk management in the South Island as they suggest that widespread damage to critical infrastructure is likely (**Robinson et al., 2015**). While the Southern Alps are sparsely populated, crucial transport links traverse them, connecting major population centres on the east coast with mining, tourism, and dairy industries on the west coast. Damage to these trans-alpine routes will severely impede access for emergency response, and have longer-term consequences for the economy and affected communities. In addition, the volume of landslide material available in many small catchments has the potential to produce debris flow hazards following the earthquake. Two years after the Wenchuan earthquake, long-duration rainfall remobilised landslide material as debris flows that killed several hundred people and buried towns by up to 5 m (**Xu et al., 2012**). Significant rainfall events are common on the west coast of the South Island where daily rainfall can exceed 350 mm. Simultaneous post-earthquake debris flows in many landslide-affected catchments are therefore likely to exacerbate the initial disaster both spatially and temporally.

5.3. Earthquake-generated erosion

Herein we have focussed solely on the coseismic erosion resulting from an Alpine Fault earthquake. Nevertheless, large earthquakes on other faults (**Fig. 1**) are also likely to contribute substantially to erosion. Following the 1929 Murchison (**Pearce and O'Loughlin, 1985**) and 1968 Inangahua (**Adams, 1981**) earthquakes, substantial erosion was recorded in the Buller catchment, while the 1929 Arthur's Pass earthquake triggered a 55 million m^3 landslide in the Taramakau catchment (**Whitehouse and Griffiths, 1983**). The 1826 Fiordland earthquake is also thought to be responsible for widespread geomorphic effects in the form of landslides and coastal dune formation in the vicinity of the Hollyford catchment (**Barnes et al., 2013; Wells and Goff, 2007**). The Hollyford river catchment as well as those north of the Taramakau are likely to sustain up to 70 years worth of annual erosion from a single Alpine Fault earthquake. With multiple earthquakes affecting these catchments between major Alpine Fault ruptures, total coseismic denudation (i.e. from all earthquake sources) may be the dominant erosional process for these catchments.

Within the central Southern Alps, Alpine Fault-derived coseismic erosion appears to play a more minor role compared to annual aseismic erosion, with coseismic denudation being equivalent to <10 years of aseismic denudation. This is likely a result of the extremely high annual rainfall and uplift rates, and consequently large *SSY* in this region (**Fig. 1**). Erosion of the Southern Alps therefore appears to be dominated by rainfall in the central section, with earthquakes playing a far larger, and perhaps dominant, role in the northern and southern sections. In those catchments dominated by coseismic erosion, Alpine Fault events may account for up to a third of total erosion.

6. Conclusions

1. Estimating the spatial extent and scale of coseismic landsliding following future large earthquakes is vital for assessing the hazards posed by such events. An M_w 8.0 earthquake on the Alpine Fault is anticipated to produce ~30,000–70,000 landslides with 68% confidence. Up to 90% of these are expected to affect a ~7,000 km^2 region along the western range-front of the Southern Alps at an average density of 2–9 landslides km^{-2}. Total landslide volumes for the scenario event are estimated to be ~0.2–1.7 km^3.
2. Sixteen order 6 and larger river catchments are identified as being most severely affected by landsliding, including all west-draining catchments in the central Southern Alps and several east-draining catchments. Of these the Taramakau, Waiho-Callery, and Hollyford catchments are anticipated to be the worst affected in terms of landslide number, producing ~10× more landslides than average for their catchment size.
3. Landsliding is expected to result in the equivalent of several decades to a century's worth of annual aseismic denudation in the northern and southern river catchments. This suggests that Alpine Fault earthquakes

account for up to a third of the total erosion in these catchments. Smaller earthquakes on other faults also affect these catchments, suggesting that earthquakes may be the dominant erosive process outside the central Southern Alps.

4. In the central Southern Alps, coseismic denudation is thought to play a more minor role compared to aseismic denudation, but is still likely to be equivalent to up to a decade of annual aseismic denudation. Rainfall and uplift are therefore likely to be the dominant erosive processes in the central Southern Alps.

Acknowledgements

We sincerely thank the two reviewers as well as Alex Densmore and Russell Blong for their thoughtful comments and suggestions on initial versions of the manuscript. We also thank Theodosios Kritikos and Susanna Jenkins for help with modelling approaches and statistical analysis. Finally we would like to thank the editor, Takashi Oguchi, for his thorough and helpful comments on various versions of the manuscript. The landslide inventories for the 2003 and 2009 Fiordland earthquakes were kindly provided by GNS Science. This work was supported by a University of Canterbury Doctoral Scholarship and the Mason Trust.

References

Adams, J. (1980) Paleoseismicity of the Alpine fault seismic gap, New Zealand, Geology, 8, 72-76.

Adams, J. (1981) Earthquake-dammed lakes in New Zealand, Geology, 9, 215-219.

Barnes, P.M., Bostock, H.C., Neil, H.L. (2013) A 2300-year paleoearthquake record of the southern Alpine Fault and Fiordland Subduction Zone, New Zealand, based on stacked turbidites. Bulletin of the Seismological Society of America 103(4): 2424-2446, doi: 10.1785/0120120314.

Barth, N.C., Boulton, C., Carpenter, B.M., Batt, G.E., Toy, V.G. (2013) Slip localization on the southern Alpine Fault, New Zealand. Tectonics 31: 1–21, doi: 10.1002/tect.20041.

Beavan, J., Denys, P., Denham, M., Hager, B., Herring, T., Molnar, P. (2010) Distribution of present-day vertical deformation across the Southern Alps, New Zealand, from 10 years of GPS data. Geophysical Research Letters 37: 7-11.

Berryman, K., Alloway, B. S., Almond, P., Barrell, D., Duncan, R. P., McSaveney, M. J., Read, S. and Tonkin, P. (2001) Alpine fault rupture and landscape evolution in Westland, New Zealand, in Proceedings 5th International Conference of Geomorphology, Tokyo.

Berryman, K.R., Cochran, U.A., Clark, K.J., Biasi, G.P., Langridge, R.M., Villamor, P. (2012) Major earthquakes occur regularly on an isolated plate boundary fault. Science, 336(6089): 1690-1693.

Biasi, G.P., Langridge, R.M., Berryman, K.R., Clark, K.J., Cochran, U. (2015) Maximum likelihood recurrence parameters and conditional probability of a ground-rupturing earthquake on the southern Alpine Fault, South Island, New Zealand. Bulletin of the Seismological Society of America 105(1): 94-107, doi: 10.1785/0120130259

Brunetti, M.T., Guzzetti, F., Rossi, M. (2009) Probability distributions of landslide volumes. Nonlinear Processes in Geophysics 16:179-188.

Bull, W. B. (1996) Prehistorical earthquakes on the Alpine fault, New Zealand, J. Geophys. Res., 101(B3), 6037-6050, doi:10.1016/0148-9062(94)92684-0.

Cogez, A., Meynadier, L., Allègre, C., Limmois, D., Herman, F., Gaillardet, J. (2015). Constraints on the role of tectonic and climate on erosion revealed by two time series analysis of marine cores around New Zealand. Earth and Planetary Science Letters, 410, 174-185.

Cooper, A.F. (1980) Retrograde Alteration of Chromian Kyanite in Metachert and Amphibolite Whiteschist from the Southern Alps, New Zealand, with Implications for Uplift on the Alpine Fault, Contributions to Mineralogy and Petrology, 75(2), 153-164, doi:10.1007/BF00389775.

Crozier, M.J. (2005) Multiple-occurrence regional landslide events in New Zealand: hazard management issues, Landslides, 2 (4), 247-256.

Davies, T.R.H. (2014) Landslide Hazards, Risks, and Disasters: Introduction. In: Landslide Hazards, Risks, and Disasters: Introduction Edited by T.R.H. Davies. Elsevier, Amsterdam, 472p

Davies, T.R.H., Korup, O. (2007) Persistent alluvial fanhead trenching resulting from large, infrequent sediment inputs, Earth Surf. Proc. Land., 32(5), 725–742, doi:10.1002/esp.

Davies, T.R.H., McSaveney, M.J. (2006) Runout of rock avalanches and volcanic debris avalanches (Invited Keynote Lecture), in Proceedings of the international conference on fast slope movements: prediction and prevention for risk mitigation, edited by L. Piceralli, Naples.

Davies, T.R.H., McSaveney, M.J., Doscher, C. (2005) Project No. 03/499 Monitoring and effects of landslide-induced aggradation in the Poerua Valley, Westland.

De Pascale, G.P., Langridge, R.M. (2012) First direct geological evidence of a great earthquake in 1717, central Alpine Fault, New Zealand. Geology.

De Pascale G.P., Quigley M., Davies T.R.H. (2014) Lidar reveals uniform Alpine Fault offsets and bimodal plate boundary rupture behaviour, New Zealand. Geology 42(5): 411-414, doi: 10.1130/G35100.1.

Del Gaudio, V., Wasowski J. (2004) Time probabilistic evaluation of seismically-induced landslide hazard in Irpinia (Southern Italy), Soil Dyn. Earthquake Eng., 24, 915–928.

Field E.H., Jordan T.H., Cornell C.A. (2003) OpenSHA: A developing community-modelling environment for seismic hazard analysis. Seismological Research Letters 74(4): 406-419.

Fry, B., Bannister, S., Beavan, J., Bland, L., Bradley, B., Cox, S., Cousins, J., Gale, N., Hancox, G. T., Holden, C., Jongens, R., Power, W., Prasetya, G., Reyners, M., Ristau, J., Robinson, R., Samsonov, S., Wilson, K., The GeoNet Team (2010) The Mw 7.6 Dusky Sound earthquake of 2009: Preliminary report. Bulletin of the New Zealand National Society of Earthquake Engineering, 43(1):24–40.

Griffiths, G.A. (1979) High sediment yields from major rivers of the Western Southern Alps, New Zealand, Nature, 282, 61-63.

Guzzetti, F., Ardizzone, F., Cardinali, M., Rossi, M., Valigi, D. (2009) Landslide volumes and landslide mobilization rates in Umbria, central Italy. Earth and Planetary Science Letters, 279(3):222–229.

Hall, L., Robinson, T. R., Duffy, B., Borella, M., Gravley, D., Hampton, S. (2014) Using landslide susceptibility modelling to investigate potential earthquake triggers for the anomalously large Green Lake rock avalanche, New Zealand. In: Geologic Society of America Conference Abstracts, October 2014, Vancouver, Canada. Geological Society of America.

Hancox, G. T., Perrin, N. (1994) Green Lake Landslide: A very large ancient rock slide in glaciated terrain, Fiordland, New Zealand. Technical Report Report 93/18, GNS Sciences.

Hancox, G. T., Cox, S., Turnbull, I. M., Crozier, M. J. (2003) Reconnaissance studies of landslides and other ground damage caused by the Mw 7.2 Fiordland earthquake of 22 August 2003. Technical Report, GNS Sciences, GNS Science Limited, Lower Hutt, New Zealand.

Hewitt, K., Clague, J. J., Orwin, J. F. (2008) Legacies of catastrophic rock slope failures in mountain landscapes, Earth-Sci. Rev., 87(1-2), 1-38, doi:10.1016/j.earscirev.2007.10.002.

Hicks, D. M., Hill, J., Shankar, U. (1996) Variation of suspended sediment yields around New Zealand: the relative importance of rainfall and geology, IAHS publication, (236), 149–156.

Howarth J.D., Fitzsimmons S.J., Norris R., Jacobsen G.E. (2012) Lake sediments record cycles of sediment flux driven by large earthquakes on the Alpine Fault, New Zealand. Geology 40(12): 1091-1094.

Howarth J.D., Fitzsimons S.J., Norris R., Jacobsen G.E. (2014) Lake sediments record high shaking that provides insights into the location and rupture length of large earthquakes on the Alpine Fault, New Zealand. Earth and Planetary Science Letters 403:340-351.

Kamp, P.J.J., Green, P.F., White, S. H. (1989) Fission track analysis reveals character of collisional tectonics in New Zealand, Tectonics, 8, 169–195.

Keefer, D.K. (1984) Landslides caused by earthquakes. , Geological Soceity of America Bulletin, 95 (4), 406-421.

Keefer, D.K. (1994) The importance of earthquake-induced landslides to long-term slope erosion and slope-failure hazards in seismically active regions, Geomorphology, 10, 265–284.

Keefer, D.K. (2000) Statistical analysis of an earthquake-induced landslide distribution – the 1989 Loma Prieta, California event, Engineering Geology, 58 (3), 231-249.

Keefer, D.K. (2002) Investigating landslides caused by earthquakes—a historical review, Surv. Geophys. 23, 473– 510.

Khazai, B., Sitar, N. (2004) Evaluation of factors controlling earthquake-induced landslides caused by the Chi-Chi earthquake and comparison with the Northridge and Loma Prieta events. Engineering Geology, 71 (1), 79-95.

Korup, O., McSaveney, M. J., Davies, T.R.H. (2004) Sediment generation and delivery from large historic landslides in the Southern Alps, New Zealand, Geomorphology, 61, 189-207, doi:10.1016/j.geomorph.2004.01.001.

Kritikos, T., Robinson, T.R., Davies, T.R.H. (2015) Regional coseismic landslide hazard assessment without historical landslide inventories: A new approach, J. Geophys. Res. Earth Surf., 120, doi:10.1002/2014JF003224.

Li, G., West, J., Densmore, A. L., Jin, Z., Parker, R. N., Hilton, R. G. (2014) Seismic mountain building: Landslides associated with the 2008 Wenchuan earthquake in the context of a generalized model for earthquake volume balance. Geochemistry, Geophysics, Geosystems, 15(4):833–844.

Malamud, B. D., Turcotte, D. L., Guzzetti, F., Reichenbach, P. (2004) Landslides, earthquakes, and erosion, Earth Planet. Sc. Lett., 229(1-2), 45-59, doi:10.1016/j.epsl.2004.10.018.

Marc, O., Hovius, N., Meunier, P., Uchida, T., Hayashi, S. (2015) Transient changes of landslide rates after earthquakes. Geology. G36961.1, doi:10.1130/G36961.1.

Miles, S.B., Keefer, D.K. (2000) Evaluation of seismic slope-performance models using a regional case study, Environ. Eng. Geosci., 6, 25–39.

Newmark, N.M. (1965), Effects of earthquakes on dams and embankments, Geotechnique, 15, 139–159.

Norris, R.J., Cooper, A.F. (2001) Late Quaternary slip rates and slip partitioning on the Alpine Fault, New Zealand, J. Struct. Geol., 23(2-3), 507-520, doi:10.1016/S0191-8141(00)00122-X.

Parker, R.N., Densmore, A.L., Rosser, N.J., de Michele, M., Li, Y., Huang, R., Whadcoat, S., Petley, D.N. (2011) Mass wasting triggered by the 2008 Wenchuan earthquake is greater than orogenic growth. Nature Geoscience, 4, DOI: 10.1038/NGEO1154.

Pearce, A.J., O'Loughlin, C.L. (1985). Landsliding during a M7.7 earthquake: influence of geology and topography. Geology, 13(12):855–858.

Rattenbury, M.S., Isaac, M.J. (2012) The QMAP 1:250 000 Geological Map of New Zealand Project. New Zealand Journal of Geology and Geophysics, 55(4):393–405.

Remondo, J., Gonzalez, A., Diaz De Terán, J.R., Cendrero, A., Fabbri, A., Chung, C.-J.F. (2003), Validation of landslide susceptibility maps; Examples and applications from a case study in northern Spain, Nat. Hazards, 30(3), 437–449.

Robinson, T.R., Davies, T.R.H. (2013) Review Article: Potential geomorphic consequences of a future great (M_w=8.0+) Alpine Fault earthquake, South Island, New Zealand. Natural Hazards and Earth Systems Science, 13, 2279-2299, DOI: 10.5194/nhess-13-2279-2013.

Robinson, T.R., Wilson, T.M., Davies, T.R.H., Orchiston, C., Thompson, J. (2014) Design and development of realistic exercise scenarios: a case study of the 2013 Civil Defence Exercise Te Ripahapa, GNS Science Miscellaneous Series 69, 113 p.

Robinson, T.R., Davies, T.R.H., Wilson, T.M., Orchiston, C., Barth, N. (2015) Evaluation of coseismic landslide hazard on the proposed Haast-Hollyford Highway, South Island, New Zealand. Georisk: Assessment and Management of Risk for Engineered Systems and Geohazards, 1-18.

Stewart, J.P., Blake, T.F., Hollingsworth, R.A. (2003), A screen analysis procedure for seismic slope stability, Earthquake Spectra, 19, 697–712.

Wellman, H. W. (1955) New Zealand Quaternary tectonics, Geol. Rundsch., 43(1), 248-257.

Wells, A., Goff, J. (2007) Coastal dunes in Westland, New Zealand, provide a record of paleoseismic activity on the Alpine fault, Geology, 35(8), 731-734.

Whitehouse, I.E., Griffiths, G.A. (1983) Frequency and hazard of large rock avalanches in the central Southern Alps, New Zealand, Geology, 11(6), 331-334.

Xu, Q., Zhang, S., Li, W. L., van Asch, T. W. J. (2012) The 13 August 2010 catastrophic debris flows after the 2008 Wenchuan earthquake, China, Nat. Hazard Earth Sys., 12(1), 201-216, doi:10.5194/nhess-12-201-2012.

Yetton, M. D. (1998) Progress in understanding the paleoseismicity of the central and northern Alpine Fault, Westland, New Zealand, New Zeal. J. Geol. Geop., 41(4), 475–483.